

Nonlinear magnetotransport in a dc-current-biased graphene

C. M. Wang^{1,*} and X. L. Lei²

¹*School of Physics and Electrical Engineering, Anyang Normal University, Anyang 455000, China*

²*Department of Physics, Shanghai Jiaotong University, 1954 Huashan Road, Shanghai 200030, China*

(Dated: February 6, 2018)

A balance-equation scheme is developed to investigate the magnetotransport in a dc-current-biased graphene. We examine the Shubnikov-de Haas oscillation under a nonzero bias current. With an increase in the current density, the oscillatory differential resistivity exhibits phase inversion, in agreement with recent experimental observation. In the presence of surface optical phonons, a second phase inversion may occur at higher dc bias, due to the reduced influence of electron-heating and the enhanced direct effect of current on differential magnetoresistivity. We also predict the appearance of current-induced magnetoresistance oscillation in suspended graphene at lower magnetic fields and larger current densities. For the graphene mobility currently available ($\approx 20 \text{ m}^2/\text{Vs}$), the oscillatory behavior may be somewhat altered by magnetophonon resonance arising from intrinsic acoustic phonon under finite bias current condition.

PACS numbers: 75.47.-m, 72.80.Vp, 73.50.Fq

I. INTRODUCTION

Since its isolation for the first time in 2004,¹ graphene, a two-dimensional (2D) single-layer of carbon atoms, has attracted an explosion of interest²⁻⁴ due to both its fundamental physics and its potential technological applications. In contrast to ordinary semiconductors, the application of a strong perpendicular magnetic field on pristine graphene results in an energetic quantization proportional to the square root of external magnetic field with the existence of a true zero-energy sharing equally by electrons and holes. As a result, magnetotransport in graphene may exhibits unusual properties. For example, the unique quantum Hall effect in graphene showing half-integer Hall plateaus,^{5,6} has become the experimental evidence of massless linear-energy fermionic excitation.

Similarly, the resistivity minima of Shubnikov-de Haas oscillation (SdHO) of graphene appears when filling factor equals $4(n + \frac{1}{2})$ with n an integer. Recently, Tan *et al.*⁷ found that in addition to the damp of oscillation due to elevated carrier temperature, a phase inversion of the differential magnetoresistivity occurs under dc bias in graphene with relatively low zero-field mobility, i.e. SdHO maxima (minima) invert to minima (maxima). They attributed the observed interesting phenomenon to the elevated electron temperature. The dominant energy dissipation they referred arises from the diffusion of hot carriers to electrodes. However, when a graphene is on a polar substrate, inelastic carrier scattering with surface optical phonons (SO phonons) is important and offers an intrinsic energy-dissipation mechanism.⁸⁻¹⁰ This notable phase-inversion effect has also been observed experimentally in usual two-dimensional electron gas (2DEG) with high mobility.¹¹ So far, a microscopic theoretical analysis including carrier-phonon scattering effect on dc-current-induced phase inversion of SdHO has still been lacking even for parabolic energy-band system.

The magnetoresistance oscillation directly induced by a dc current, periodic in current density and in inverse

magnetic field, is another noteworthy nonlinear transport phenomenon, which was first observed a decade ago in conventional 2DEG.^{12,13} The effect is ascribed to the Zener tunneling between Hall-field-tilted Landau levels due to short-range (SR) impurity scattering.^{12,14} Later, by including inelastic phonon scattering, a microscopic balance-equation scheme has been constructed, conveniently accounting for this current-induced nonlinear transport phenomenon with considering the electron heating.¹⁵ So far, however, investigations of nonlinear magnetoresistance oscillation have been carried out only for high-mobility 2DEGs with parabolic energy dispersion.¹²⁻¹⁷ Owing to the absence of much of extrinsic impurities and SO phonons, the suspended graphene can achieve relatively high mobility^{18,19} that Landau levels can be well resolved even in quite a weak magnetic field. Hence, it is expected that this kind of nonlinear magnetoresistance oscillation could be observed in suspended graphene. Therefore, an efficient scheme capable of dealing with magnetotransport in graphene under an external current bias is in sore need.

The balance-equation approach, which is especially suitable to deal with current-controlled nonlinear transport, was established based on the separation of the center-of-mass motion from the relative carrier motion in parabolic energy-band systems.²⁰⁻²⁴ It turns out that this scheme can be applied to systems with linear energy dispersion.²⁵ In this paper, we will generalize this scheme to graphene subject to a magnetic field and a finite dc current. The paper is organized as follows. In Sec. II, the force- and energy-balance equations are derived for graphene in the presence of normal magnetic field and external dc current. The effect of a finite dc bias on the SdHO in a graphene on a SiO_2 substrate is investigated in Sec. III A. The current-control magnetoresistance oscillation in a suspended graphene is discussed in Sec. III B. A summary is given in Sec. IV. The derivation of energy-balance equation is presented in Appendix.

II. BALANCE-EQUATION FORMULATION

We consider a single layer graphene in the x - y plane under the influence of a uniform magnetic field $\mathbf{B} = B\hat{z}$ along the z direction and a dc electric field $\mathbf{E} = (E_x, E_y)$ applied in the layer plane. The carriers having enough density near the K or K' points in the graphene, are interacting with each other, coupled with lattice vibrations of the graphene as well as the oxide interface, and scattered by randomly located disorders. The Hamiltonian of this system consists of an carrier part \mathcal{H}_e , a phonon part \mathcal{H}_{ph} , and carrier-impurity and carrier-phonon interactions \mathcal{H}_{ei} and \mathcal{H}_{ep} :

$$\mathcal{H} = \mathcal{H}_e + \mathcal{H}_{ph} + \mathcal{H}_{ei} + \mathcal{H}_{ep}. \quad (1)$$

Here, the carrier Hamiltonian can be written as

$$\mathcal{H}_e = \sum_{j,\alpha} [v_F(\pi_j^x \sigma_j^x + c_\alpha \pi_j^y \sigma_j^y) + e\mathbf{r}_j \cdot \mathbf{E}], \quad (2)$$

where $\mathbf{r}_j = (x_j, y_j)$, $\mathbf{p}_j = (p_{jx}, p_{jy})$, $\boldsymbol{\pi}_j \equiv \mathbf{p}_j + e\mathbf{A}(\mathbf{r}_j) = (\pi_j^x, \pi_j^y)$, and $\boldsymbol{\sigma}_j = (\sigma_j^x, \sigma_j^y, \sigma_j^z)$, stand, respectively, for the coordinate, momentum, canonical momentum, and Pauli operators of the j th carrier in the pseudospin space formed by the A and B sublattices; c_α is a valley-related coefficient equaling $+1$ or -1 for carrier in $\alpha = K$ or K' valley; $\mathbf{A}(\mathbf{r}) = (-By, 0)$ is the vector potential of the magnetic field in the Landau gauge; $v_F = 1.1 \times 10^6$ m/s is the Fermi velocity. The forms of \mathcal{H}_{ei} and \mathcal{H}_{ep} are similar to those given in Refs. 23 and 24, without intervalley transition of carriers.

In the frame work of balance equation approach,^{20–22} we introduce the 2D center-of-mass (c.m.) momentum and coordinate $\mathbf{P}_\alpha = \sum_{j \in \alpha} \mathbf{p}_j$ and $\mathbf{R}_\alpha = N_\alpha^{-1} \sum_{j \in \alpha} \mathbf{r}_j$, and the relative-carrier momenta and coordinates $\mathbf{p}'_j = \mathbf{p}_j - \mathbf{P}_\alpha/N_\alpha$ and $\mathbf{r}'_j = \mathbf{r}_j - \mathbf{R}_\alpha$ for carriers in the α valley having carrier number N_α , to write the Hamiltonian \mathcal{H}_e into the sum of a single-particle c.m. part $\mathcal{H}_{cm} = \sum_\alpha \mathcal{H}_{cm}^\alpha$ and a many-particle relative-carrier part $\mathcal{H}_{er} = \sum_\alpha \mathcal{H}_{er}^\alpha$: $\mathcal{H}_e = \mathcal{H}_{cm} + \mathcal{H}_{er}$, with

$$\mathcal{H}_{cm}^\alpha = v_F(\Pi_x^\alpha \sigma_{\alpha c}^y + c_\alpha \Pi_y^\alpha \sigma_{\alpha c}^x) + N_\alpha e \mathbf{E} \cdot \mathbf{R}_\alpha, \quad (3)$$

$$\mathcal{H}_{er}^\alpha = \sum_{j \in \alpha} [v_F(\pi_j'^x \sigma_j^y + c_\alpha \pi_j'^y \sigma_j^x)]. \quad (4)$$

In this, $\boldsymbol{\Pi}^\alpha \equiv \mathbf{P}_\alpha + N_\alpha e \mathbf{A}(\mathbf{R}_\alpha) = (\Pi_x^\alpha, \Pi_y^\alpha)$ is the center-of-mass canonical momentum of the α valley and $\boldsymbol{\pi}'_j \equiv \mathbf{p}'_j + e\mathbf{A}(\mathbf{r}'_j) = (\pi_j'^x, \pi_j'^y)$ is the canonical momentum for the j th relative carrier. Here we have also introduced c.m. spin operators $\sigma_{\alpha c}^x \equiv N_\alpha^{-1} \sum_{j \in \alpha} \sigma_j^x$ and $\sigma_{\alpha c}^y \equiv N_\alpha^{-1} \sum_{j \in \alpha} \sigma_j^y$ for the α valley. The commutation relations between the c.m. Pauli operators $\sigma_{\alpha c}^x$ and $\sigma_{\alpha c}^y$ and the Pauli operators σ_j^x and σ_j^y of the j th carrier are of order of $1/N_\alpha$. Therefore, for a macroscopically large N_α system, the c.m. part \mathcal{H}_{cm} actually commutes with the relative-carrier part \mathcal{H}_{er} in the Hamiltonian, i.e. the c.m. motion and the relative motion of

carriers are truly separated from each other. The couplings between the two emerge only through the carrier-impurity and carrier-phonon interactions. Furthermore, the electric field \mathbf{E} shows up only in \mathcal{H}_{cm} . And, in view of $[r'_{i\beta_1}, p'_{j\beta_2}] = i\delta_{\beta_1\beta_2}(\delta_{ij} - 1/N_\alpha) \simeq i\delta_{\beta_1\beta_2}\delta_{ij}$, i.e. the relative-carrier momenta and coordinates can be treated as canonical conjugate variables, the relative-motion part \mathcal{H}_{er}^α is just the Hamiltonian of N_α carriers in the α valley of graphene in the magnetic field without electric field.

In terms of the c.m. coordinate \mathbf{R}_α and the relative carrier density operator $\rho_q^\alpha = \sum_{j \in \alpha} e^{i\mathbf{q} \cdot \mathbf{r}'_j}$, the carrier-impurity and carrier-phonon interactions can be written as^{21,22}

$$\mathcal{H}_{ei} = \sum_{\alpha, \mathbf{q}, a} U(\mathbf{q}) e^{i\mathbf{q} \cdot (\mathbf{R}_\alpha - \mathbf{r}_a)} \rho_q^\alpha, \quad (5)$$

$$\mathcal{H}_{ep} = \sum_{\alpha, \mathbf{q}, \nu} M(\mathbf{q}, \nu) \varphi_{\mathbf{q}\nu} e^{i\mathbf{q} \cdot \mathbf{R}_\alpha} \rho_q^\alpha. \quad (6)$$

Here $U(\mathbf{q})$ and $M(\mathbf{q}, \nu)$ are, respectively, the impurity potential (an impurity at randomly distributed position \mathbf{r}_a) and carrier-phonon coupling matrix element in the plane-wave representation, and $\varphi_{\mathbf{q}\nu} \equiv b_{\mathbf{q}\nu}^\dagger + b_{-\mathbf{q}\nu}^\dagger$ is the phonon field operator with $b_{\mathbf{q}\nu}^\dagger$ and $b_{\mathbf{q}\nu}$ being the creation and annihilation operators for a 2D phonon of wavevector \mathbf{q} in the branch ν having frequency $\Omega_{\mathbf{q}\nu}$.

The derivation of balance equations starts by noticing that the c.m. velocity (operator) \mathbf{V}_α is the time variation of its coordinate: $\mathbf{V}_\alpha = \dot{\mathbf{R}}_\alpha = -i[\mathbf{R}_\alpha, \mathcal{H}] = v_F(\sigma_{\alpha c}^y \hat{i} + c_\alpha \sigma_{\alpha c}^x \hat{j})$, and proceeds from the Heisenberg equations for the rate of change of the center-of-mass canonical momentum $\dot{\mathbf{P}}_\alpha = -i[\mathbf{P}_\alpha, \mathcal{H}]$, and that of the relative-carrier energy $\dot{\mathcal{H}}_{er}^\alpha = -i[\mathcal{H}_{er}^\alpha, \mathcal{H}]$. The statistical average of the above operator equations can be determined to linear order in the carrier-impurity and carrier-phonon interactions \mathcal{H}_{ei} and \mathcal{H}_{ep} using the initial density matrix $\hat{\rho}_0 = Z^{-1} e^{-\mathcal{H}_{ph}/T} e^{-\mathcal{H}_{er}/T_e}$ with lattice temperature T and a common carrier temperature T_e for carriers in both valleys in view of the symmetry of graphene band structure, which give rise to equal carrier number densities $N_K = N_{K'}$ and equal average c.m. velocities $\mathbf{v} = \mathbf{v}_\alpha = \langle \mathbf{V}_\alpha \rangle$ ($\alpha = K, K'$).

Steady-state transport balance equations are obtained by setting $\sum_\alpha \langle \dot{\mathbf{P}}_\alpha \rangle = 0$ and $\sum_\alpha \langle \dot{\mathcal{H}}_{er}^\alpha \rangle = 0$. The derived force and energy balance equations, which are identical for both valleys, can be written (for graphene system of unit area) as

$$0 = -N e \mathbf{v} \times \mathbf{B} - N e \mathbf{E} + \mathbf{f}_i + \mathbf{f}_p, \quad (7)$$

$$0 = (\mathbf{f}_i + \mathbf{f}_p) \cdot \mathbf{v} + w. \quad (8)$$

Derivation of energy-balance equation is given in appendix. Here $N = \sum_\alpha N_\alpha$ is the total number density of carriers (in both valleys) for system of unity area, \mathbf{f}_i and \mathbf{f}_p are total frictional forces experienced by the center of

mass due to impurity and phonon scatterings:

$$\mathbf{f}_i = n_i \sum_{\mathbf{q}} |U(\mathbf{q})|^2 \mathbf{q} \Pi_2(\mathbf{q}, \omega_0), \quad (9)$$

$$\begin{aligned} \mathbf{f}_p = \sum_{\mathbf{q}, \nu} |M(\mathbf{q}, \nu)|^2 \mathbf{q} \Pi_2(\mathbf{q}, \Omega_{\mathbf{q}\nu} + \omega_0) \\ \times \left[n\left(\frac{\Omega_{\mathbf{q}\nu}}{T}\right) - n\left(\frac{\Omega_{\mathbf{q}\nu} + \omega_0}{T_e}\right) \right], \end{aligned} \quad (10)$$

and w is the rate of carrier energy-dissipation to the lattice due to carrier-phonon interactions:

$$\begin{aligned} w = \sum_{\mathbf{q}, \nu} |M(\mathbf{q}, \nu)|^2 \Omega_{\mathbf{q}\nu} \Pi_2(\mathbf{q}, \Omega_{\mathbf{q}\nu} + \omega_0) \\ \times \left[n\left(\frac{\Omega_{\mathbf{q}\nu}}{T}\right) - n\left(\frac{\Omega_{\mathbf{q}\nu} + \omega_0}{T_e}\right) \right]. \end{aligned} \quad (11)$$

In these equations n_i is the impurity density, $n(x) = (e^x - 1)^{-1}$ is the Bose distribution function, $\omega_0 \equiv \mathbf{q} \cdot \mathbf{v}$, $\Pi_2(\mathbf{q}, \omega) = \sum_{\alpha} \Pi_2^{\alpha}(\mathbf{q}, \omega)$ with $\Pi_2^{\alpha}(\mathbf{q}, \omega)$ standing for the imaginary part of the Fourier spectrum of the relative-carrier density correlation function of the α valley in the magnetic field defined by

$$\Pi^{\alpha}(\mathbf{q}, t - t') = -i \theta(t - t') \langle [\rho_{\mathbf{q}}^{\alpha}(t), \rho_{-\mathbf{q}}^{\alpha}(t')] \rangle_0, \quad (12)$$

where $\rho_{\mathbf{q}}^{\alpha}(t) = e^{i \mathcal{H}_{\text{ert}} t} \rho_{\mathbf{q}}^{\alpha} e^{-i \mathcal{H}_{\text{ert}} t}$ and $\langle \dots \rangle_0$ denotes the statistical averaging over the initial density matrix $\hat{\rho}_0$.^{20,24}

In the magnetic field the imaginary part of the relative-carrier density correlation function $\Pi_2(\mathbf{q}, \omega)$ can be calculated in the Landau representation.²⁶ The eigenstates of the single-particle Hamiltonian $h^{\alpha} = v_F(\pi^x \sigma^x + c_{\alpha} \pi^y \sigma^y)$ in the magnetic field $B \hat{z}$ can be specified by a set of quantum numbers $\{n, k_x, \sigma, \lambda, \alpha\}$ with n, k_x, σ , and λ denoting the Landau index, the x component of the wave vector, the pseudospin index, and the band index (electron $\lambda = 1$ or hole $\lambda = -1$), respectively. The eigenenergies of h^{α} are

$$\varepsilon_{\lambda n} = \lambda v_F \sqrt{2eBn} = \lambda \varepsilon_n \quad (n = 0, 1, 2, \dots), \quad (13)$$

which is pseudospin- and valley-degenerate. The corresponding eigenfunctions can be written as $\Psi_{n k_x \sigma}^{\alpha \lambda} = \psi_{n k_x}^{\alpha \lambda} \otimes \chi_{\sigma}$ with χ_{σ} standing for the eigenstate of Pauli matrix σ_z and

$$\psi_{n k_x}^{K \lambda}(\mathbf{r}) = \frac{e^{i k_x x}}{\sqrt{1 + s_n}} \begin{pmatrix} -\lambda s_n \phi_{n-1, k_x}(y) \\ \phi_{n, k_x}(y) \end{pmatrix}, \quad (14)$$

$$\psi_{n k_x}^{K' \lambda}(\mathbf{r}) = \frac{e^{i k_x x}}{\sqrt{1 + s_n}} \begin{pmatrix} \phi_{n, k_x}(y) \\ -\lambda s_n \phi_{n-1, k_x}(y) \end{pmatrix}. \quad (15)$$

Here $s_n = 1 - \delta_{n,0}$ and $\phi_{n, k_x}(y)$ is the harmonic oscillator eigenfunction:

$$\phi_{n, k_x}(y) = \frac{1}{\sqrt{2^n n! l_B \sqrt{\pi}}} \exp\left[-\frac{(y - y_c)^2}{2 l_B^2}\right] H_n\left(\frac{y - y_c}{l_B}\right), \quad (16)$$

with $H_n(x)$ the Hermite polynomial, $l_B = \sqrt{1/(eB)}$ and $y_c = k_x/(eB)$.

The $\Pi_2(\mathbf{q}, \omega)$ can be expressed in the Landau-representation in the form^{25,27,28}

$$\Pi_2(\mathbf{q}, \omega) = \frac{g_s g_v}{2\pi l_B^2} \sum_{\substack{n, n' \\ \lambda, \lambda'}} C_{n, n'}^{\lambda, \lambda'} \left(\frac{l_B^2 q^2}{2}\right) \Pi_2(n, n'; \lambda, \lambda'; \omega), \quad (17)$$

$$\begin{aligned} \Pi_2(n, n'; \lambda, \lambda'; \omega) = -\frac{1}{\pi} \int d\epsilon [f(\epsilon) - f(\epsilon + \omega)] \\ \times \text{Im} G_{\lambda n}(\epsilon + \omega) \text{Im} G_{\lambda' n'}(\epsilon). \end{aligned} \quad (18)$$

Note that despite different forms of wave functions the $\Pi_2(n, n'; \lambda, \lambda'; \omega)$ function and the transform factor $C_{n, n'}^{\lambda, \lambda'}(l_B^2 q^2/2)$ are identical for both valleys and for both pseudospin directions, whence the valley and spin summations just give rise to the multiplication of degenerate constants $g_v = g_s = 2$. Here the transform factor

$$\begin{aligned} C_{n, n'}^{\lambda, \lambda'}(x) = \frac{x^{n_2 - n_1} e^{-x}}{(1 + s_n)(1 + s_{n'})} \frac{n_1!}{n_2!} \left[L_{n_1}^{n_2 - n_1}(x) \right. \\ \left. + \lambda \lambda' s_n s_{n'} \sqrt{\frac{n_2}{n_1}} L_{n_1 - 1}^{n_2 - n_1}(x) \right]^2, \end{aligned} \quad (19)$$

with $n_1 = \min(n, n')$, $n_2 = \max(n, n')$, and $L_n^m(x)$ being associated Laguerre polynomials.

The Landau levels are broadened due to impurity, phonon and carrier-carrier scatterings. We model the imaginary part of the retarded Green's function $\text{Im} G_{\lambda n}(\epsilon)$ in Eq.(18), or the density-of-state (DOS) of the λn th Landau level, using a Gaussian form²⁹

$$\text{Im} G_{\lambda n}(\epsilon) = -\frac{\sqrt{2\pi}}{\Gamma_{\lambda n}} \exp\left[-\frac{2(\epsilon - \varepsilon_{\lambda n})^2}{\Gamma_{\lambda n}^2}\right], \quad (20)$$

with a half-width³⁰

$$\Gamma_{\lambda n} = [2\omega_{\lambda n}/(\pi\tau_s)]^{1/2}, \quad (21)$$

where τ_s is the single-particle lifetime and $\omega_{\lambda n} = |\varepsilon_{\lambda n+1} - \varepsilon_{\lambda n}|$ is the level distance or the cyclotron frequency of the λn th Landau level, with $\omega_{\lambda n} \approx v_F(eB/2n)^{1/2} = eBv_F^2/\varepsilon_n$ for large n irrespective of the band index, giving rise to valley- and band-independent broadening $\Gamma_{\lambda n} = \Gamma_n$.

In the following we restrict ourselves to the n -doped case at relatively low temperature, i.e., the carriers are electrons, that we only need to consider states with band index $\lambda = 1$. For conciseness we will no longer write out the band index λ in the expressions and equations and denote $\Pi_2(n, n'; 1, 1; \omega)$, $C_{n, n'}^{1, 1}(x)$, and $\text{Im} G_{1n}(\epsilon)$ simply as $\Pi_2(n, n'; \omega)$, $C_{n, n'}(x)$ and $\text{Im} G_n(\epsilon)$. The Landau-level summation indices n and n' in all the equations are taken over $0, 1, 2, \dots$ but the $\text{Im} G_0(\epsilon)$ function should be replaced by $\text{Im} G_0^p(\epsilon) = \theta(\epsilon) \text{Im} G_0(\epsilon)$ due to electron-hole symmetry of the band structure.²⁵

The total electron number density N is related to the chemical potential ε_f of the Landau quantized graphene system by the equation

$$N = -\frac{g_s g_v}{2(\pi l_B)^2} \sum_n \int d\epsilon f(\epsilon) \text{Im} G_n(\epsilon), \quad (22)$$

in which $f(\epsilon) = \{\exp[(\epsilon - \varepsilon_f)/T_e] + 1\}^{-1}$ is the Fermi distribution function at electron temperature T_e .

Force- and energy-balance equations (7) and (8), in which the frictional forces \mathbf{f}_i , \mathbf{f}_p and the electron dissipation rate w are functions of carrier drift velocity \mathbf{v} and electron temperature T_e , describe the steady-state nonlinear magnetotransport in the graphene. With given carrier drift velocity \mathbf{v} or the dc current density $\mathbf{J} = Ne\mathbf{v}$, the electron temperature T_e can be determined by the energy-balance equation, and the magnetoresistance is obtained from force-balance equation. Note that the frictional forces \mathbf{f}_i and \mathbf{f}_p are in the opposite direction of the drift velocity \mathbf{v} and their magnitudes are functions of $v = |\mathbf{v}|$ only: $\mathbf{f}_i = -v\mathbf{f}_i(v)/v$ and $\mathbf{f}_p = -v\mathbf{f}_p(v)/v$. In the Hall configuration, e.g. with a drift velocity $\mathbf{v} = (v, 0)$ in the x direction, the force-balance equation Eq. (7) yields a transverse resistivity $R_{xy} = -E_y/(Ne v) = -B/(Ne)$, a longitudinal resistivity $R_{xx} = -E_x/(Ne v) = -(f_i + f_p)/(N^2 e^2 v)$, and a longitudinal differential resistivity $r_{xx} = -(N^2 e^2)^{-1} d(f_i + f_p)/dv$.

III. NUMERICAL CALCULATIONS AND DISCUSSIONS

We will use a phenomenological parameter α_F to relate the single particle lifetime τ_s to the transport scattering time in the system:³¹ $\tau_{tr} = \alpha_F \tau_s$, and, by expressing τ_{tr} with the zero-field mobility μ ,^{32,33} we can write the Landau-level broadening in the vicinity of Fermi energy $\varepsilon_F = v_F \sqrt{\pi N}$ as

$$\Gamma = (ev_F/\pi)[2B\alpha_F/(N\mu)]^{1/2}. \quad (23)$$

The broadening parameter will be taken to be $\alpha_F = 2$ throughout the calculation.

We consider two cases: a graphene monolayer on a SiO₂ substrate⁷ and a suspended monolayer graphene. The electrons in graphene are scattered by charged impurities distributed at a distance d from the layer with $d = 4 \text{ \AA}$ for the graphene on SiO₂ substrate and $d = 0$ for the suspended one, having a scattering potential

$$U(\mathbf{q}) = \frac{Ze^2}{2\epsilon_0 \kappa_{\text{avg}} q} e^{-qd}. \quad (24)$$

Here κ_{avg} is the average dielectric constant of two regions (air and SiO₂ or air) surrounding the graphene. Hence^{34,35} $\kappa_{\text{avg}} \approx (1 + \kappa)/2 = 2.45$ for non-suspended graphene ($\kappa = 3.9$ is the static dielectric constant of SiO₂), while $\kappa_{\text{avg}} \approx 1$ for suspended one.

For intrinsic acoustic phonon scatterings in the graphene layer, there are two 2D modes, the sum of which

can be treated as isotropic one^{36,37} with a scattering matrix element

$$|M(\mathbf{q}, \text{AC})|^2 = \frac{D^2 q}{2\rho_m v_{\text{ph}}}, \quad (25)$$

and an averaged sound velocity³⁸ $v_{\text{ph}} = 2 \times 10^4 \text{ m/s}$. We choose the deformation potential constant as a moderate value^{38,39} $D = 19 \text{ eV}$ and the mass density $\rho_m = 7.6 \times 10^{-8} \text{ g/cm}^2$.³⁸

The electrons can also be scattered by the intrinsic optical phonons in graphene. However, the energies of these intrinsic optical modes are greater than 150 meV ($\approx 1740 \text{ K}$), which is much larger than the lattice and electron temperatures concerned and can be neglected. For graphene on the SiO₂ substrate, the surface optic phonon couples to the electrons in graphene by an effective electric field. Due to small van der Waals distance between the polar substrate and the interface, the 2D surface optical (SO) phonon plays a more prominent role in transport in graphene than in usual heterojunctions. The coupling matrix element can be written as⁸

$$|M(\mathbf{q}, \text{SO})|^2 = \frac{e^2 \Omega_{\text{so}}}{2\epsilon_0 q} \left(\frac{1}{\kappa_{\infty} + 1} - \frac{1}{\kappa + 1} \right) e^{-2qd}, \quad (26)$$

where Ω_{so} is the frequency of SO phonon and κ_{∞} is the optical dielectric constant of substrate. For SiO₂, $\kappa_{\infty} = 2.4$ and there are two SO-phonon modes having frequencies³⁵ $\Omega_{\text{so}}^{(1)} = 59 \text{ meV}$ and $\Omega_{\text{so}}^{(2)} = 155 \text{ meV}$. The second mode is negligible in the present study owing to its large frequency.

A. SdHO under nonzero dc current

In order to study the SdHO under a finite bias dc current in graphene we calculate the magnetoresistivity of a graphene monolayer on a SiO₂ substrate having electron density $N = 3.16 \times 10^{12} \text{ cm}^{-2}$ and zero-magnetic-field mobility $\mu = 0.8 \text{ m}^2/\text{Vs}$ in the magnetic fields ranging from 0 to 15 T at lattice temperature $T = 2 \text{ K}$ on the basis of balance equations (7) and (8). The calculated longitudinal magnetoresistivity R_{xx} and differential magnetoresistivity r_{xx} are shown in Fig. 1(a) and Fig. 1(b) as functions of the magnetic field B for different given current densities J . The standard SdHO curves of graphene are obtained, where the valleys of magnetoresistivity R_{xx} locate at the magnetic fields corresponding to the half-integer filling factors^{5,7} $\nu = \frac{2\pi N}{eB} = 4(n + \frac{1}{2})$ with $n = 2, 3, 4, \dots$, as indicated in the figure. The increasing current density suppresses the oscillation, while the peak/valley positions remain essentially unchanged. The significant feature of current-related SdHO appears in the differential resistivity as shown in Fig. 1(b). With the rise of current density, the oscillation of differential resistivity r_{xx} not only tends to decrease its amplitude, but, more prominently, exhibits phase inversion, e.g., SdHO minima (maxima) invert to maxima (minima) at certain

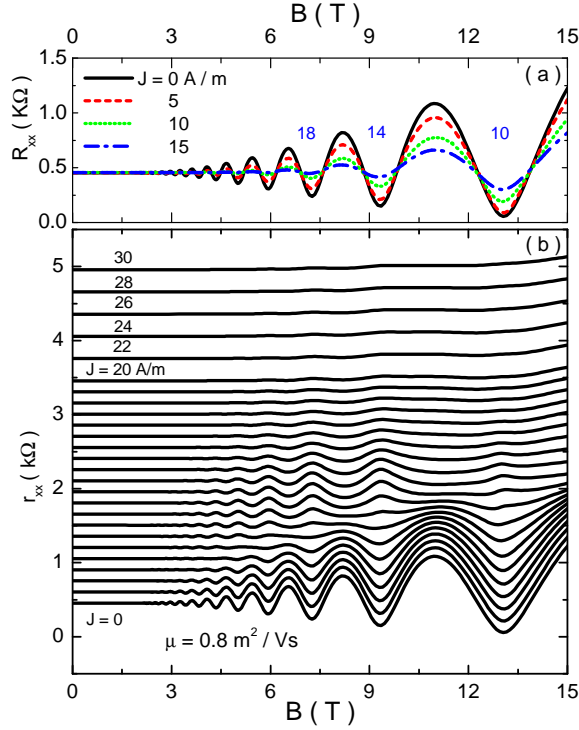


FIG. 1: (Color online) (a) Magnetoresistivity R_{xx} is shown versus magnetic field B at various dc current densities $J = 0, 5, 10, 15$ A/m. The integers near the valleys indicate the filling factors. (b) Differential magnetoresistivity r_{xx} is plotted as a function of the magnetic field for various current densities at lattice temperature $T = 2$ K. These r_{xx} curves of different J values are vertically offset for clarity. The current densities are $J = 0, 1, 2, \dots, 20$ A/m in 1 A/m step for the lower 21 ones, or are indicated in the figure for others. The system is a monolayer graphene on a SiO_2 substrate having electron density $N = 3.16 \times 10^{12} \text{ cm}^{-2}$ and zero-magnetic-field mobility $\mu = 0.8 \text{ m}^2/\text{Vs}$.

value of bias current density, which is roughly linearly dependent on the magnetic field of the SdHO extrema. These features are in good agreement with the experimental observation.⁷

The phase inversion of SdHO is closely related to the rise of electron temperature with increasing bias current. Fig. 2 shows the calculated electron temperature T_e as a function of the bias current density J at magnetic field strengths $B = 6, 8$, and 10 T (a), as well as T_e versus B at current densities $J = 5, 10, 15, 20$ A/m (b). When current density is lower than 12 A/m, the electron temperature almost linearly depends on the dc bias. For higher current density, the enhanced energy dissipation arising from electron-SO-phonon interaction restrains the linear increase of electron temperature. In the fixed bias current case (b), only a small oscillation of electron temperature around a certain value shows up for almost the whole magnetic field range presented in the figure.

In the balance-equation scheme, the frictional forces f_i and f_p are functions of the drift velocity v (i.e. the

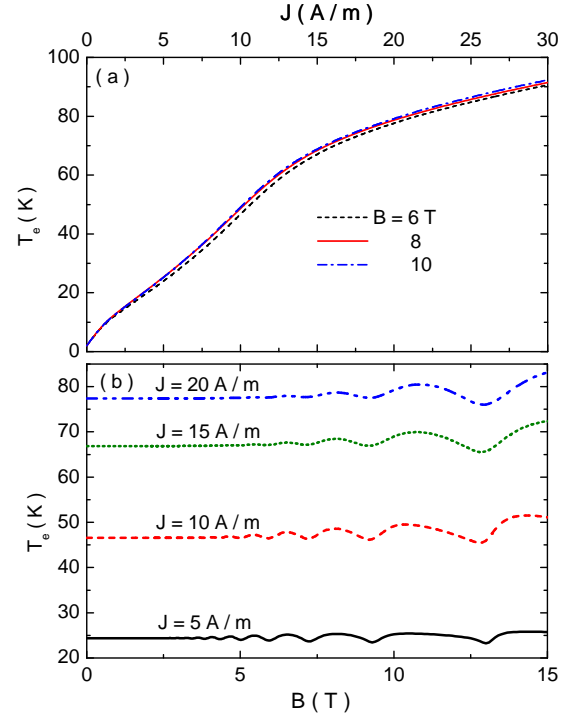


FIG. 2: (Color online) Electron temperature T_e is shown as a function of dc bias current density at various magnetic fields (a) and as a function of magnetic field at various bias current densities (b) for the same system as described in Fig. 1.

current density $J = Nev$) and the electron temperature T_e , and the latter is determined as a function of v from the energy balance equation. Therefore the differential resistivity derived can be expressed as

$$\begin{aligned} r_{xx} &= R_{xx} + J \frac{\partial R_{xx}}{\partial T_e} \frac{\partial T_e}{\partial J} + J \frac{\partial R_{xx}}{\partial J}, \\ &= R_{xx} + r_{xx}^{T_e} + r_{xx}^v, \end{aligned} \quad (27)$$

where $r_{xx}^{T_e}$ can be thought as the part arising from the electron-temperature change and r_{xx}^v as that direct from current-density change. We plot the calculated R_{xx} , $r_{xx}^{T_e}$ and r_{xx}^v , as well as the total r_{xx} , as functions of the magnetic field B for several bias current densities $J = 4, 8, 12, 16$, and 20 A/m in Fig. 3. The three constituent parts R_{xx} , $r_{xx}^{T_e}$ and r_{xx}^v all exhibit oscillations having extrema at positions $\nu = 4(n + \frac{1}{2})$. However, the phase of $r_{xx}^{T_e}$ is opposite to those of R_{xx} and r_{xx}^v . Note that in the current range $0 < J < 12$ A/m, when SO-phonons play a relatively small role in dissipating energy, the electron temperature grows almost linearly with increasing current density and $|r_{xx}^v|$ is one order of magnitude smaller than $|R_{xx}|$ or $|r_{xx}^{T_e}|$, hence, R_{xx} and $r_{xx}^{T_e}$ constitute dominant contributions to total r_{xx} and the current-induced electron temperature rising accounts for the phase inversion of r_{xx} in this current density regime, as pointed out by Tan *et al.*⁷

With further increase in the current density, R_{xx} de-

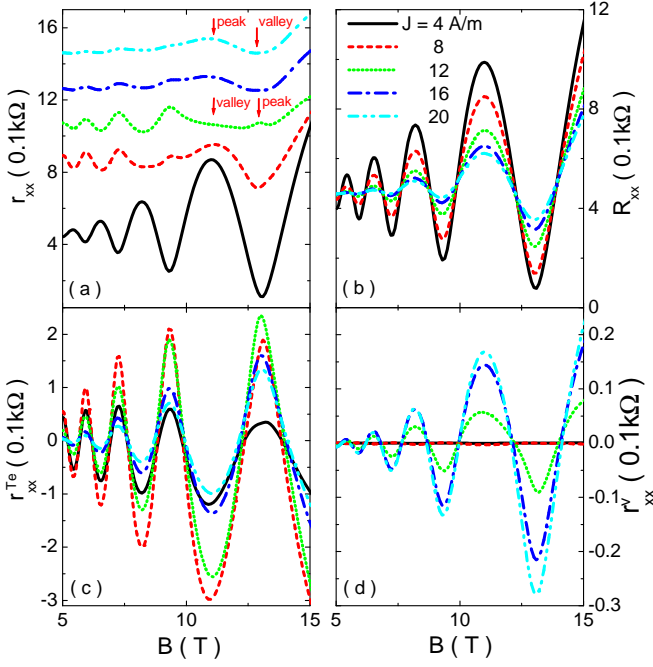


FIG. 3: (Color online) Differential magnetoresistivity r_{xx} (a), and its constituent parts R_{xx} (b), $r_{xx}^{T_e}$ (c) and r_{xx}^v (d) defined in (27), are shown versus magnetic field for various bias current densities $J = 4, 8, 12, 16, 20$ A/m. The r_{xx} curves in (a) are vertically offset for clarity.

creases, while $r_{xx}^{T_e}$ first ascends and then descends in view of the slowdown of the electron temperature increase due to the enhanced role of SO-phonon scattering. On the other hand, at higher current density J , the current direct-contributed part, r_{xx}^v , also becomes non-negligible. This could give rise to a second phase-inversion of r_{xx} oscillation. It can be seen in Fig. 3(a) that the peak (valley) at low current density near 11 T (13 T) first inverts to valley (peak) and then changes back to peak (valley) with the rise of dc bias.

B. Current-induced magnetoresistance oscillation

We turn to the regime of lower magnetic fields, where the SdHO hardly shows up.

In the case of low temperature $T_e \ll \varepsilon_F$ and large filling factor $\nu = \frac{\pi N}{2eB} \gg 1$, the major contribution to the summation in the density correlation function (17) comes from Landau levels near the Fermi energy, i.e., terms $n \simeq n' \sim \nu$, and then the function $C_{n,n'}(x)$ has a sharp principal maximum near $x \sim 4\nu$. Therefore, as a function of the in-plane momentum q , the $\Pi_2(\mathbf{q}, \omega)$ function given in (17) sharply peaks around $q \approx 2k_F$, with $k_F = \sqrt{\pi N}$ being the Fermi wave vector. In the case of a finite drift velocity v , the motion of the center-of-mass provides the relative electron with an additional energy $\omega_0 = \mathbf{q} \cdot \mathbf{v}$ during its transition from a state to another state having

a momentum change of \mathbf{q} , as shown in the expressions of (9), (10) and (11) for \mathbf{f}_i , \mathbf{f}_p and w . The sharp peaking of $\Pi_2(\mathbf{q}, \omega)$ function around $q \approx 2k_F$ indicates that most effective processes contributing to the magnetoresistance come from those electron transitions which involve an additional energy around $\omega_j = 2k_F v$. Looking at electron transitions in the Landau representation, we can see that the transition rate is proportional to the overlap of the DOS of the related two Landau levels around the Fermi surface, $\text{Im}G_n(\epsilon + \omega_j)\text{Im}G_{n'}(\epsilon)$, and the maximum overlap occurs at $\varepsilon_n - \varepsilon_{n'} = \omega_j$. Thus, the impurity-induced longitudinal magnetoresistivity may show extrema when $\varepsilon_{\nu+l} - \varepsilon_\nu \approx l\omega_B = \pm\omega_j$ with $l = 0, \pm 1, \pm 2, \dots$ and $\omega_B = eBv_F/k_F$ being the distance of the neighboring Landau levels in the vicinity of Fermi surface. Therefore, the impurity-related magnetoresistivity would exhibit a periodical oscillation when changing drift velocity v or changing magnetic field B . This current-induced magnetoresistance oscillation (CIMO) is characterized by a dimensionless parameter ω_j/ω_B with a period $\Delta(\omega_j/\omega_B) \approx 1$: when ω_j/ω_B varies by a unity value, the magnetoresistivity experiences change of an oscillatory period.

As an example, Fig. 4 displays the calculated magnetoresistivity and differential magnetoresistivity versus ω_j/ω_B for fixed bias current densities $J = 40, 50$ and 60 A/m (a) or for fixed magnetic fields $B = 0.2, 0.3$ and 0.4 T (b) at lattice temperature $T = 2$ K in a suspended monolayer graphene having electron density $N = 3.16 \times 10^{12} \text{ cm}^{-2}$ and linear mobility $\mu = 20 \text{ m}^2/\text{Vs}$, assuming Coulombic impurity scattering potential (24) with $d = 0$. The longitudinal magnetoresistivity R_{xx} (plotted in the insets) shows relatively weak oscillations, while the differential magnetoresistivity r_{xx} exhibits marked oscillations, having an approximate period $\Delta(\omega_j/\omega_B) \approx 1$ in both cases. Notable magnetoresistance oscillations appear in the well-resolved Landau level regime when $2\Gamma \leq \omega_B$, or $B \geq 8\alpha_F/\pi\mu \approx 0.25$ T, and the enhanced current weakens the oscillation amplitude due to the rising electron temperature.

Note that the parameter $\omega_j/\omega_B = (2\pi/e^2 v_F)(J/B)$ characterizing the CIMO depends only on the band-dispersion related v_F for systems of linear energy band, thus the periodic behavior of CIMO is universal in graphene in terms of J/B , irrespective of carrier-density N . This situation is in contrast to the conventional 2DEG of parabolic band,¹⁵ where the Fermi velocity v_F involved in the characterizing parameter depends on the carrier density, so does the periodicity of the magnetoresistance oscillation in it.

The basic features of the oscillatory R_{xx} and r_{xx} are: oscillation amplitude decays with increasing ω_j/ω_B but enhances with increasing current density or magnetic field strength in the discussed range. In the fixed current density case of Fig. 4(a), where the electron temperature has only weak change with changing magnetic field, the amplitude decrease of the resistance oscillation is due to the enlarged overlap of neighboring Landau lev-

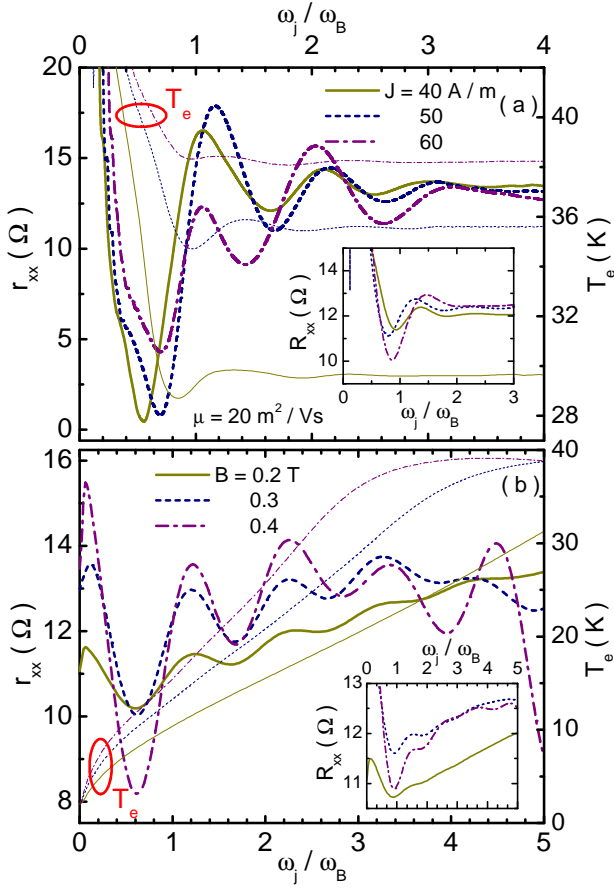


FIG. 4: (Color online) Differential magnetoresistivity r_{xx} , electron temperature T_e and magnetoresistivity R_{xx} (inset) are shown as functions of ω_j/ω_B for various fixed dc current densities $J = 40, 50, 60$ A/m (a) and for various fixed magnetic fields $B = 0.2, 0.3, 0.4$ T (b). The system is a suspended monolayer graphene having electron density $N = 3.16 \times 10^{12} \text{ cm}^{-2}$ and zero-magnetic-field mobility $\mu = 20 \text{ m}^2/\text{Vs}$ at lattice temperature $T = 2$ K, with Coulombic impurity potential (24) of $d = 0$.

els with decreasing magnetic field. In the fixed B -field case of Fig. 4(b), the electron temperature grows when increasing bias current density, resulting in the suppression of the resistance oscillation. Nevertheless, the oscillation amplitude shown in these figures exhibits somewhat anomalous behavior, especially around the first peak of $J = 60$ A/m curve in Fig. 4(a) and the last peak of $B = 0.4$ T curve in Fig. 4(b). These r_{xx} anomalies come from the contribution of phonon-related differential resistivity r_{ph} .

In contrast to the case of high-mobility 2DEG,¹⁵ the electron temperature T_e in the present monolayer graphene may reach the range of 40 K in the case of high current density $J \geq 60$ A/m and the magnitude of phonon-related resistivity may not be negligible in comparison with impurity contribution as shown in Fig. 5(a) and (c), where the constituent parts of r_{xx} in the mono-

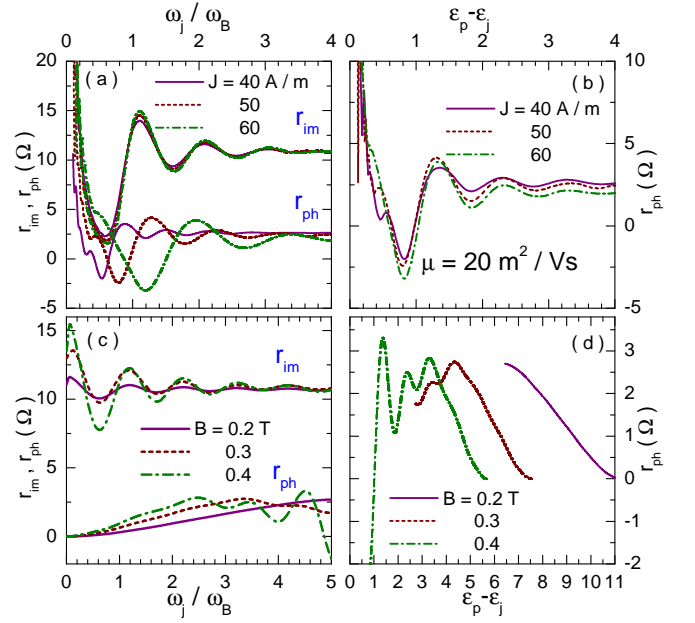


FIG. 5: (Color online) Impurity-related and phonon-related differential resistivities r_{im} and r_{ph} are shown versus ω_j/ω_B for fixed current densities $J = 40, 50, 60$ A/m (a) or fixed magnetic fields $B = 0.2, 0.3, 0.4$ T (c). Phonon-related differential resistivity r_{ph} is replotted as a function of $\varepsilon_p - \varepsilon_j$ for fixed current densities (b) or fixed magnetic fields (d).

layer graphene, the resistivity $r_{im} = -(N^2 e^2)^{-1} df_i/dv$ due to impurity scattering and the resistivity $r_{ph} = -(N^2 e^2)^{-1} df_p/dv$ due to intrinsic acoustic phonon scattering, are plotted as functions of ω_j/ω_B respectively for the cases of fixed current density (a) and for the cases of fixed magnetic field strength (c). The oscillation behavior of r_{im} closely follows the basic feature of CMO, but r_{ph} , though generally smaller in magnitude, appears quite different. In the fixed current case the marked drop of r_{ph} around $\omega_j/\omega_B \sim 1$ [Fig. 5(a)] leads to the descent of the first peak of r_{xx} at $J = 60$ A/m curve in Fig. 4(a). In the fixed magnetic field case, the resonant peak of r_{ph} around $\omega_j/\omega_B \sim 4.5$ for $B = 0.4$ T [Fig. 5(c)] gives rise to the enhancement and position shift of the last peak of r_{xx} in Fig. 4(b).

Such kind of oscillatory r_{ph} is referred to the magnetophonon resonance induced by acoustic phonons. As in conventional 2DEGs,^{40–42} acoustic phonon-related resistivity r_{ph} in a dc biased graphene should feature a periodic appearance of resonant peaks with respect to $\varepsilon_p - \varepsilon_j$ axis, where $\varepsilon_j \equiv \omega_j/\omega_B$ and $\varepsilon_p \equiv \omega_{ph}/\omega_B$ are the ratios of the energy ω_j provided by the drifting center-of-mass and the energy $\omega_{ph} = 2k_F v_{ph}$ provided by the optimum phonons to the inter-Landau-level distance ω_B of electron near the Fermi surface. We replot the phonon-related resistivities r_{ph} given in Fig. 5(a) and (c) as a function of $\varepsilon_p - \varepsilon_j$ in Fig. 5(b) and (d). They indeed show peaks near integer positions $\varepsilon_p - \varepsilon_j \approx l = 1, 2, 3$ and 4, indicating electron scattered resonantly across l Landau-level

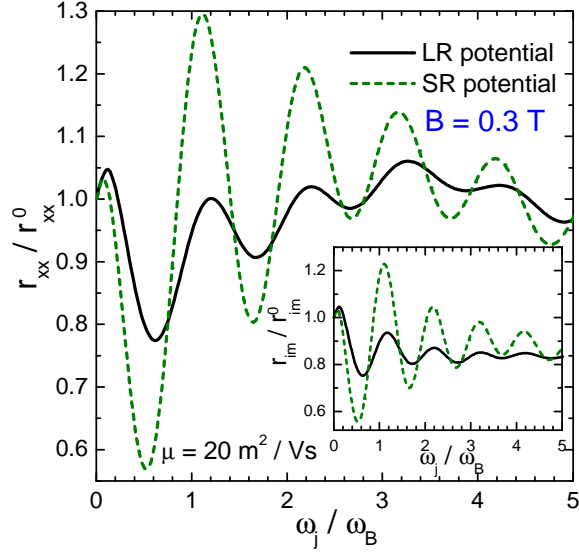


FIG. 6: (Color online) Normalized differential resistivity versus ω_j/ω_B at fixed magnetic field $B = 0.3$ T for the system subject to LR or SR impurity-scattering. The inset displays normalized impurity-related differential resistivity r_{im} . Here r_{xx}^0 and r_{im}^0 are total and impurity-related differential resistivity in the absence of magnetic field. The zero-magnetic-field mobility $\mu = 20 \text{ m}^2/\text{Vs}$.

spacings by absorbing or emitting an optimum acoustic phonon under the biased dc current condition. At low magnetic fields, the magnetophonon resonance in r_{ph} can not be seen in the range shown, because of weakened oscillation in the DOS and higher orders of resonant peaks required (e.g., $\varepsilon_p - \varepsilon_j \geq 6$ for $0 \leq \varepsilon_j \leq 5$ at $B = 0.2$ T).

Analogous to the case of 2DEG,^{31,43} the amplitude of current-controlled magnetoresistance oscillation depends strongly on the correlation length of electron-impurity scattering potential, though the oscillation periods are essentially the same in terms of ε_j . To see this, we plot the normalized total and impurity-induced differential resistivities, r_{xx} and r_{im} , for Coulombic impurity scattering potential (24) with $d = 0$ (LR) and short-range (SR) disorders (assuming same zero-magnetic-field mobility $\mu = 20 \text{ m}^2/\text{Vs}$ and $\alpha_{\Gamma} = 2$ for both cases) in Fig. 6 as functions of ω_j/ω_B at fixed magnetic field $B = 0.3$ T. The lattice defects in graphene are usually modeled by SR impurities. It is seen that both r_{xx} and r_{im} display much stronger oscillations in the case of SR potential than that of LR potential, but the maxima and minima positions are almost identical in both cases.

IV. SUMMARY

In summary, we have presented an investigation of non-linear magnetotransport in graphene under a finite dc bias at low temperature employing a balance-equation scheme appropriate to systems with linear-energy dis-

person. In the relatively strong magnetic field range when SdHO controlled by the filling factor $\nu = 2\pi N/eB$ shows up we find that the oscillatory differential magnetoresistivity exhibits phase inversion with rising bias current density, in agreement with recent experimental finding. Further, it is demonstrated that electron-SO-phonon scattering is important for graphene on a polar substrate, which suppresses the rapid increase of electron temperature and may result in a second phase inversion of the oscillatory resistance. In the lower magnetic field and higher bias current density regime when SdHO becomes weak a CIMO is appreciable in suspended graphene. It appears markedly in the differential resistivity when Landau levels are still well resolved and is controlled by the parameter $\varepsilon_j = (2\pi/e^2 v_F)(J/B)$ having approximate period $\Delta\varepsilon_j \sim 1$. For the graphene mobility available today ($\approx 20 \text{ m}^2/\text{Vs}$), the oscillatory behavior may be somewhat altered by magnetophonon resonance induced by intrinsic acoustic phonon under finite bias current. We hope this current-controlled magnetoresistance oscillation could be observed experimentally in the near future.

ACKNOWLEDGMENTS

This work was supported by the National Basic Research Program of China (Grant No. 2012CB927403), the National Science Foundation of China (Grant No. 11104002), the Program for Science&Technology Innovation Talents in Universities of Henan Province (Grant No. 2012HASTIT029), and the Program of Young Key Teachers of University in Henan Province (Grant No. 2011GGJS-148).

Appendix: Derivation of the energy-balance equation

Here we detail the derivation of the energy-balance equation for graphene. In the second quantization representation of the creation (annihilation) operators $c_{\alpha\lambda n k_x s}^\dagger$ ($c_{\alpha\lambda n k_x s}$), the relative-carrier Hamiltonian has the form:

$$\mathcal{H}_{\text{er}} = \sum_{\alpha, \lambda, n, k_x, s} \varepsilon_{\lambda n} c_{\alpha\lambda n k_x s}^\dagger c_{\alpha\lambda n k_x s} \quad (28)$$

The rate of change of the energy of relative carrier system is obtained from the Heisenberg equation of motion:

$$\begin{aligned} \dot{\mathcal{H}}_{\text{er}} &= -i[\mathcal{H}_{\text{er}}, \mathcal{H}] \\ &= - \sum_{\mathbf{q}, a} U(\mathbf{q}, z_a) e^{i\mathbf{q} \cdot (\mathbf{R} - \mathbf{r}_a)} \frac{d\rho_{\mathbf{q}}(t)}{dt} \\ &\quad - \sum_{\mathbf{q}, \nu} M(\mathbf{q}, \nu) e^{i\mathbf{q} \cdot \mathbf{R}} \varphi_{\mathbf{q}\nu}(t) \frac{d\rho_{\mathbf{q}}(t)}{dt}. \end{aligned} \quad (29)$$

Here the particle density operator

$$\rho_{\mathbf{q}}(t) = \sum_{\substack{\alpha, s, \lambda, n, k_x \\ \alpha', s', \lambda', n', k'_x}} \langle \Psi_{nk_x s}^{\alpha \lambda} | e^{i\mathbf{q} \cdot \mathbf{r}} | \Psi_{n'k'_x s'}^{\alpha' \lambda'} \rangle e^{i(\varepsilon_{\lambda n} - \varepsilon_{\lambda' n'})t} \\ \times c_{\alpha \lambda n k_x s}^\dagger c_{\alpha' \lambda' n' k'_x s'} \quad (30)$$

After statistical average of the operator equation (29), the energy-balance equation is given by²⁴

$$\frac{dU}{dt} = \left\langle \frac{d\mathcal{H}_{\text{er}}}{dt} \right\rangle = I_1 + I_2, \quad (31)$$

with

$$I_1 = i \int_{-\infty}^t dt' n_i \sum_{\mathbf{q}} |U(\mathbf{q})|^2 e^{i\mathbf{q} \cdot [\mathbf{R}(t) - \mathbf{R}(t')]} \\ \times \left\langle \left[\frac{d\rho_{\mathbf{q}}(t)}{dt}, \rho_{-\mathbf{q}}(t') \right] \right\rangle_0, \quad (32)$$

$$I_2 = i \int_{-\infty}^t dt' \sum_{\mathbf{q}, \nu} |M(\mathbf{q}, \nu)|^2 e^{i\mathbf{q} \cdot [\mathbf{R}(t) - \mathbf{R}(t')]} \\ \times \left\langle \left[\varphi_{\mathbf{q}\nu}(t) \frac{d\rho_{\mathbf{q}}(t)}{dt}, \varphi_{-\mathbf{q}\nu}(t') \rho_{-\mathbf{q}}(t') \right] \right\rangle_0. \quad (33)$$

The first integral I_1 can be simplified as

$$I_1 = - \int_{-\infty}^{\infty} dt' n_i \sum_{\mathbf{q}} |U(\mathbf{q})|^2 e^{i\mathbf{q} \cdot \mathbf{v}(t-t')} \frac{d}{dt} \Pi(\mathbf{q}, t - t') \\ - i \sum_{\mathbf{q}} |U(\mathbf{q})|^2 \langle [\rho_{\mathbf{q}}(t), \rho_{-\mathbf{q}}(t)] \rangle_0. \quad (34)$$

Here the relative-carrier density correlation function $\Pi(\mathbf{q}, t - t') = -i\theta(t - t') \langle [\rho_{\mathbf{q}}(t), \rho_{-\mathbf{q}}(t')] \rangle_0$. The second term of the above equation equals zero and the first term becomes $-\mathbf{f}_i \cdot \mathbf{v}$ after integration by parts, hence we obtain $I_1 = -\mathbf{f}_i \cdot \mathbf{v}$. Similarly, the integral $I_2 = -\mathbf{f}_p \cdot \mathbf{v} - w$. Therefore, the energy-balance equation is written as

$$\frac{dU}{dt} = \left\langle \frac{d\mathcal{H}_{\text{er}}}{dt} \right\rangle = -(\mathbf{f}_i + \mathbf{f}_p) \cdot \mathbf{v} - w. \quad (35)$$

* cmwangs@sjtu@gmail.com

- ¹ K. S. Novoselov, A. K. Geim, S. V. Morozov, D. Jiang, Y. Zhang, S. V. Dubonos, I. V. Grigorieva, and A. A. Firsov, *Science* **306**, 666 (2004).
- ² A. K. Geim and K. S. Novoselov, *Nat. Mat.* **6**, 183 (2007).
- ³ S. D. Sarma, S. Adam, E. H. Hwang, and E. Rossi, *Rev. Mod. Phys.* **83**, 407 (2011).
- ⁴ M. O. Goerbig, *Rev. Mod. Phys.* **83**, 1193 (2011).
- ⁵ Y. Zhang, Y. Tan, H. Stormer, and P. Kim, *Nature* **438**, 201 (2005).
- ⁶ K. S. Novoselov, A. K. Geim, S. V. Morozov, D. Jiang, M. I. Katsnelson, I. V. Grigorieva, S. V. Dubonos, and A. A. Firsov, *Nature* **438**, 197 (2005).
- ⁷ Z. Tan, C. Tan, L. Ma, G. T. Liu, L. Lu, and C. L. Yang, *Phys. Rev. B* **84**, 115429 (2011).
- ⁸ S. Fratini and F. Guinea, *Phys. Rev. B* **77**, 195415 (2008).
- ⁹ X. Li, E. A. Barry, J. M. Zavada, M. B. Nardelli, and K. W. Kim, *Appl. Phys. Lett.* **97**, 082101 (2010).
- ¹⁰ W. Zhu, V. Perebeinos, M. Freitag, and P. Avouris, *Phys. Rev. B* **80**, 235402 (2009).
- ¹¹ N. R. Kalmanovitz, A. A. Bykov, S. Vitkalov, and A. I. Toropov, *Phys. Rev. B* **78**, 085306 (2008).
- ¹² C. L. Yang, J. Zhang, R. R. Du, J. A. Simmons, and J. L. Reno, *Phys. Rev. Lett.* **89**, 076801 (2002).
- ¹³ A. A. Bykov, J. Q. Zhang, S. Vitkalov, A. K. Kalagin, and A. K. Bakarov, *Phys. Rev. B* **72**, 245307 (2005).
- ¹⁴ W. Zhang, H. S. Chiang, M. A. Zudov, L. N. Pfeiffer, and K. W. West, *Phys. Rev. B* **75**, 041304 (2007).
- ¹⁵ X. L. Lei, *Appl. Phys. Lett.* **90**, 132119 (2007).
- ¹⁶ J. Q. Zhang, S. Vitkalov, A. A. Bykov, A. K. Kalagin, and

- A. K. Bakarov, *Phys. Rev. B* **75**, 081305 (2007).
- ¹⁷ M. G. Vavilov, I. L. Aleiner, and L. I. Glazman, *Phys. Rev. B* **76**, 115331 (2007).
- ¹⁸ K. I. Bolotin, K. J. Sikes, Z. Jiang, M. Klima, G. Fudenberg, J. Hone, P. Kim, and H. L. Stormer, *Solid State Commun.* **146**, 351 (2008).
- ¹⁹ K. I. Bolotin, K. J. Sikes, J. Hone, H. L. Stormer, and P. Kim, *Phys. Rev. Lett.* **101**, 096802 (2008).
- ²⁰ X. L. Lei and C. S. Ting, *Phys. Rev. B* **32**, 1112 (1985).
- ²¹ X. L. Lei, J. L. Birman, and C. S. Ting, *J. Appl. Phys.* **58**, 2270 (1985).
- ²² W. Cai, X. L. Lei, and C. S. Ting, *Phys. Rev. B* **31**, 4070 (1985).
- ²³ X. L. Lei, D. Y. Xing, M. Liu, C. S. Ting, and J. L. Birman, *Phys. Rev. B* **36**, 9134 (1987).
- ²⁴ X. L. Lei, *Balance equation approach to electron transport in semiconductors* (World Scientific, Singapore, 2008).
- ²⁵ C. M. Wang and X. L. Lei, *Phys. Rev. B* **86**, 035442 (2012).
- ²⁶ C. S. Ting, S. C. Ying, and J. J. Quinn, *Phys. Rev. B* **16**, 5394 (1977).
- ²⁷ R. Roldán, J.-N. Fuchs, and M. O. Goerbig, *Phys. Rev. B* **80**, 085408 (2009).
- ²⁸ P. K. Pyatkovskiy and V. P. Gusynin, *Phys. Rev. B* **83**, 075422 (2011).
- ²⁹ T. Ando, A. B. Fowler, and F. Stern, *Rev. Mod. Phys.* **54**, 437 (1982).
- ³⁰ Y. Zheng and T. Ando, *Phys. Rev. B* **65**, 245420 (2002).
- ³¹ X. L. Lei and S. Y. Liu, *Phys. Rev. Lett.* **91**, 226805 (2003); *Phys. Rev. B*, **72**, 075345 (2005).
- ³² E. H. Hwang, S. Adam, and S. Das Sarma, *Phys. Rev.*

- Lett. **98**, 186806 (2007).
- ³³ C. M. Wang and F. J. Yu, Phys. Rev. B **84**, 155440 (2011).
- ³⁴ A. Konar, T. Fang, and D. Jena, Phys. Rev. B **82**, 115452 (2010).
- ³⁵ Massimo V. Fischetti, Deborah A. Neumayer, and E. A. Cartier, J. Appl. Phys. **90**, 4587 (2001).
- ³⁶ V. Perebeinos and P. Avouris, Phys. Rev. B **81**, 195442 (2010).
- ³⁷ R. Kim, V. Perebeinos, and P. Avouris, Phys. Rev. B **84**, 075449 (2011).
- ³⁸ E. H. Hwang and S. Das Sarma, Phys. Rev. B **77**, 115449 (2008).
- ³⁹ J. Chen, C. Jang, S. Xiao, M. Ishigami, and M. Fuhrer, Nat. Nanotechnol. **3**, 206 (2008).
- ⁴⁰ M. A. Zudov, I. V. Ponomarev, A. L. Efros, R. R. Du, J. A. Simmons, and J. L. Reno, Phys. Rev. Lett. **86**, 3614 (2001).
- ⁴¹ W. Zhang, M. A. Zudov, L. N. Pfeiffer, and K. W. West, Phys. Rev. Lett. **100**, 036805 (2008).
- ⁴² X. L. Lei, Phys. Rev. B **77**, 205309 (2008).
- ⁴³ X. L. Lei, Mater. Sci. Eng. R, **70**, 126 (2010).